Becker, D., Cailleau, B., Kaiser, D., Dahm, T. (2014): Macroscopic Failure Processes at Mines Revealed by Acoustic Emission (AE) Monitoring. - *Bulletin of the Seismological Society of America*, *104*, 4, p. 1785-1801.

DOI: http://doi.org/10.1785/0120130286

Bulletin of the Seismological Society of America, Vol. 104, No. 4, pp. 1785–1801, August 2014, doi: 10.1785/0120130286

Ⓔ

# Macroscopic Failure Processes at Mines Revealed by Acoustic Emission (AE) Monitoring

by D. Becker, B. Cailleau, D. Kaiser, and T. Dahm

**Abstract** Mining activity may cause different types of seismicity and rock failure. Typical events include (1) fully induced microearthquakes in close proximity to galleries and human activity due to high-stress concentrations (border fractures) and (2) triggered earthquakes within the rock mass at larger distance to the source of the stress perturbation (inner fractures). Type 1 is important to understand the development of rock bursts and evaluate the stability of the mine. Type 2 may be associated with larger events releasing pre-existing stress and being triggered by stress changes due to the mining operation. They are important to assess the seismic hazard related to mining activity.

To analyze these different failure processes, we use a dataset of high-frequency acoustic emission (AE) events monitored in an abandoned salt mine. The process of fracture formation in the rock mass was enhanced by the backfilling of a cavity. Thermal stresses induced by the backfilling operation are modeled with a finite-element approach, and observed AE activity is used to quantify the mechanism of event triggering in terms of a Coulomb failure model.

Two observations are outstanding. First, the instantaneous triggering of enhanced activity and the slow growth of an inner fracture in relatively far distance to the backfilled cavity is detected. The structure already showed AE activity before the refilling started and was triggered by traction-like stress transfer. Its AE activity correlates well with the calculated Coulomb stress changes at the beginning of backfilling. Second, the sudden occurrence of a macroscopic, induced border fracture at the backfilled gallery which is oriented in agreement with the acting stress field is observed. Although AE activity at the inner fracture was triggered by tiny Coulomb stress changes, indicating a structure already in critical state, formation of the border fracture required significantly larger stresses, hinting at a previously intact rock volume.

*Online Material:* Figure depicting the variability of the static Coulomb stress changes on the inner fracture for different rake values.

## Introduction

In the mining environment, ongoing human activities such as the removal of large volumes of material modify the Coulomb stress field and either promote or hinder failure in intact rock or on pre-existing slip interfaces already preloaded by the background stress field. In the border region of mined-out cavities, induced Coulomb stress changes lead to a large number of brittle failure events, sometimes expressed as rockfalls or rockbursts (e.g., Gibowicz and Kijko, 1994; Richardson and Jordan, 2002). These events are termed "border fractures" in this paper and pose a considerable risk to life and property (e.g., Young *et al.*, 1992; Ge, 2005). Most of the microseismic (MS) and acoustic emission (AE) events observed in the mining environment are linked to such failure processes in the excavation damage zone close to the cavities, as well as in the regions in the immediate vicinity of cavities (e.g., Gibowicz and Kijko, 1994; Richardson and Jordan, 2002). Apart from these events, which are often interpreted as failure due to quasi-static stress changes resulting from excavation activity, events at larger distance from the cavities also are observed (here defined as inner fractures; see also Richardson and Jordan, 2002). These events do not necessarily migrate with the advancing excavation front but are temporally and spatially distributed throughout the active mining area. They are interpreted as slip events in pre-existing shear zones activated by the stress perturbations caused by the mining activity.

To better understand the characteristics of such MS or AE events in the mining environment and their response to stress changes, several extensive studies have been carried out during the last about two decades. Such studies were conducted in underground laboratories like the Canadian Underground Research Laboratory (URL; e.g., Falls and Young, 1998; Young and Collins, 1999) and the Swedish Hard Rock Laboratory (HRL; e.g., Anderson and Martin, 2009; Andersson *et al.*, 2009), as well as in active mines such as the deep South African gold mines (e.g., Richardson and Jordan, 2002; Naoi *et al.*, 2011) or European ore (e.g., Oye *et al.*, 2005) and coal mines (e.g., Gibowicz and Kijko, 1994). Additionally, monitoring programs to mitigate risks during the active mining process are carried out by the operators of the mine (e.g., Gibowicz, 1989; Gibowicz and Kijko, 1994; Trifu, 2002; Trifu, 2010). The aim of this monitoring is to identify regions that may be susceptible to rockbursts or structural damage (e.g., Young *et al.*, 1992; Ge, 2005) or to decide when a safe re-entry to the mine is possible after a rockburst or larger event (e.g., Vallejos and McKinnon, 2011).

In the area of AE events, Naoi *et al.* (2011) studied more than 20,000 aftershocks of an **M** 2 event in a South African gold mine and identified a narrow rupture surface with an orientation that obeys the Coulomb failure criterion. They observed an Omori-type decay of the event rate in spatially distinct clusters in agreement with the idea of aftershock behavior and enhanced aftershock activity close to cavities, presumably due to stress concentrations and the existence of excavation damage zones. In the Swedish HRL, Andersson *et al.* (2009) investigated the response of a pillar to the combined effect of excavation- and thermal-induced stresses. They observed a correlation between thermal-induced tangential stresses and daily event rates for AE events close to the borehole wall, as well as the activation of a mapped shear zone within the rock pillar between the two boreholes. Practically, all these events were observed within a distance of 1 m or even less from the boreholes.

The occurrence of these brittle failure events is often explained with the concept of the Coulomb failure criterion, originally developed for natural seismicity (e.g., King *et al.*, 1994; Stein, 1999). In the case of natural seismicity, the Coulomb failure stress is either induced on a fault due to static stress changes caused by other earthquakes (e.g., King *et al.*, 1994; Stein, 1999; Freed, 2005) or to slower deformational processes in its surrounding, such as magmatic intrusions or plate deformations (e.g., Dieterich *et al.*, 2000; Toda *et al.*, 2002). If the fault is already in a critical state close to failure, even small positive changes in the Coulomb failure stress have the potential to trigger activity. However, to test the validity of these models and to obtain quantitative estimates, a precise knowledge of the spatiotemporal evolution of the stress field and large event datasets are necessary, but these are rarely available in studies dealing with natural seismicity.

In this study, a high-quality catalog of AE events spanning an extended time interval of several years and comprising tens of thousands of events in the region of interest is utilized to study the spatiotemporal evolution of microcracking activity, illuminating a pre-existing inner fracture. Coulomb stresses calculated with a 2D finite-element (FE) thermoelastic model are able to explain many features of the observed AE activity of this inner fracture, as well as those of a newly created border fracture.

## Study Site and Monitoring Network

The study site is located in the former Morsleben salt mine in northern Germany, which is used as a repository for weak to medium radioactive waste. Details on the Morsleben repository and its geologic and tectonic setting are given in Behlau and Mingerzahn (2001), Preuss *et al.* (2002), and Federal Office for Radiation Protection (2009). The salt deposits consist of highly folded Zechstein salt (z2–4) with interspersed blocks of broken anhydrite (z3HA) and other layers of deposited material with varying material parameters (e.g. carnallitite [z2SF]). These different units cover a wide range of possible deformational behaviors from brittle to very ductile and vary greatly with respect to their compressive and tensile yield stresses. In order to mitigate possible risks due to sudden mass movements in the mining complex, an extensive monitoring program is in place that records the AE and other activity in selected areas of the mining complex (Fig. 1).

Because of the ongoing creep of the salt body, AE events are ubiquitous in the study region. This microcracking either takes place along grain boundaries or breaks through grains in the salt or at the contact between different geologic units, such as rock salt and anhydrite, that serve as localized zones of weakness (e.g., Spies and Eisenblätter, 1999; Spies and Eisenblätter, 2001; Fahland *et al.*, 2005). The dataset used in this study was recorded by a network of 24 AE receivers (Fig. 1), which were installed in the early 1990s and span a volume of roughly $80 \times 80 \times 50$ m at a depth of about 300 m below the surface. However, due to the low damping of the seismic signals in salt, which is on the order of a few dB per 10 m travel path (Eisenblätter and Spies, 2000), the monitored region is significantly larger. AE events in the mine are located automatically with a triggering approach, and only event parameters such as hypocenter, origin time, automatically determined *P*- and *S*-wave onsets, and maximum amplitude are saved in a log file. (The waveforms are not routinely retained; see Spies and Eisenblätter, 2001, Köhler *et al.*, 2009, and Becker *et al.*, 2010, for specifics of the recording system and the localization procedure.) Data are sampled with 200 kHz, and the main signal energy is in the 1–20 kHz frequency range. From empirical energy relations (Eisenblätter and Spies, 2000), moment magnitudes in the $-6$ to $-4$ $M_w$ range are estimated for the dB magnitude range from 40 to 80 (corresponding to an AE magnitude, $M_{AE}$, range of 2–4) observed for most of the events in this study (e.g., Maghsoudi *et al.*, 2013). Completeness of the AE catalog was studied in detail by Becker *et al.* (2010) and Maghsoudi *et al.* (2013). Although the AE catalog is incomplete

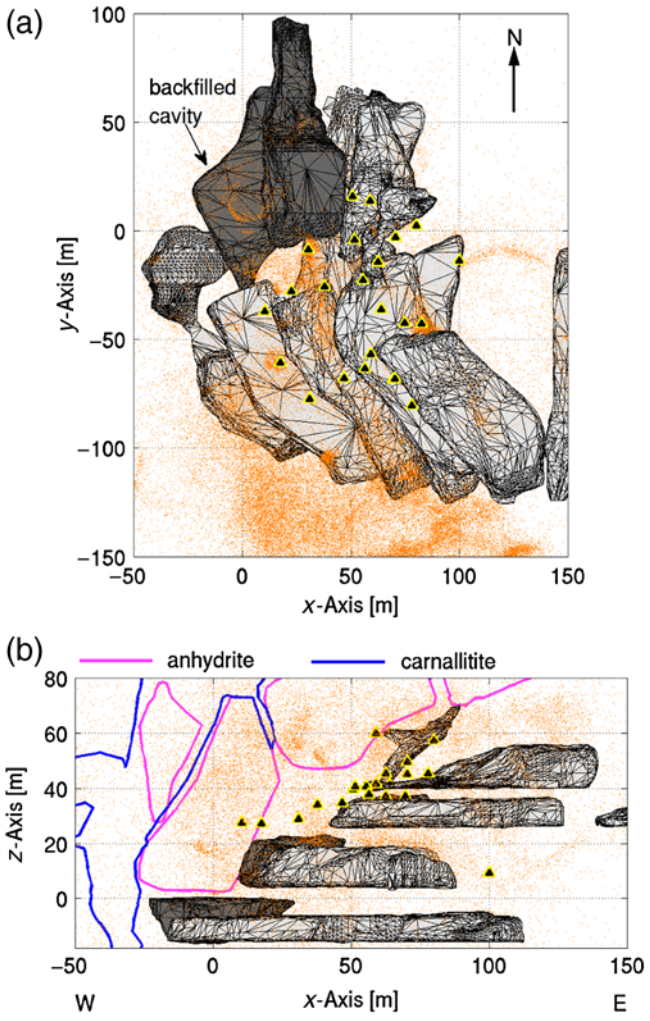


**Figure 1.** (a) The distribution of cavities (dark gray outlines indicate cavities depicted in later figures), locations of acoustic emission (AE) receivers (triangles), and distribution of AE activity with magnitude ≥52 dB (i.e., $M_{AE} \geq 2.6$) during the two years before the start of backfilling (dots). (b) The east–west cross section at $y = 0$, showing the distribution of anhydrite blocks and carnallitite seams in the study site. Intersections of geologic units indicate uncertainty in the precise determination of the boundaries. The cavities, AE events, and AE receivers depicted in (a) are projected onto the cross section. The color version of this figure is available only in the electronic edition.

during times of working activity in the mine, it is complete during times of strongest AE activity, with up to 400 events per hour studied in detail in this paper.

In order to increase the structural stability of the mining complex, selected cavities were backfilled with salt concrete. The first cavity to be subjected to this procedure was instrumented with a temperature chain anchored between the top and the floor of the cavity. This backfilled cavity is located slightly toward the west and below the network of AE receivers (Fig. 1), which results in a slightly reduced magnitude range of the AE catalog when compared to the center of the AE network. Nevertheless, the location accuracy for well-located AE events is on the order of 1–2 m (Becker *et al.*, 2010), and the number of events recorded in the vicinity of the cavity is high enough for a detailed analysis of microcracking processes in this area (Köhler *et al.*, 2009; Becker *et al.*, 2010).

In the backfilling process, liquid salt concrete at ambient temperature is pumped into the target cavity, where it starts to solidify. During this curing process of the concrete, large amounts of heat are released and transferred to the surrounding rock mass (Fig. 2). The addition of new, colder (with respect to the solidifying material) concrete during the next working period again reduces the temperature in the cavity. Because of this cyclic nature of the backfilling process, with five consecutive days of backfilling activity interrupted by two days (weekend) without working activity, the temperature at the ceiling of the backfilled cavity also exhibits a cyclic character. This in turn induces cyclic thermal stressing in the surrounding rock mass. The whole backfilling process, during which a total volume of about 26,000 $m^3$ of salt concrete was pumped into the target cavity, lasted 182 days. The relative temperature increase during the work-free two-day interval reached values of up to 8° C for the last heating period before backfilling was completed (178–180 days after start of backfilling), whereas these values were on the order of 2° C during the start of backfilling (days 20–40 of backfilling). Daily temperature fluctuations at the top of the cavity during the five-day working period increased from about 0.5° C at the beginning of backfilling to about 3° C toward the end due to the decreasing distance from the ceiling to the surface of the backfilling material. From day 91 up to day 105, a two-week interruption (Christmas holidays) in backfilling activity is evidenced by a slowly decreasing temperature profile (Fig. 2).

Because of the fast decay of the thermal signal with growing distance from the cavity, a more gradual loading history is expected for the rock mass at distances exceeding a few meters from the gallery. However, thermal stresses induced in the rock mass consist of a superposition of a body-force-like and a surface-traction-like term (e.g., Berger, 1975; Ben-Zion and Leary, 1986; Prawirodirdjo *et al.*, 2006). Although the body-force-like term is due to the thermal expansion at a given point and travels with the slow velocity of the thermal front, the traction-like term is due to elastic coupling of thermal expansion at distant points and is instantaneously transmitted over large distances (Ben-Zion and Leary, 1986). Thus, even at a distance of 10–30 meters from the backfilled cavity, a cyclic stress component is expected and might find its expression in the weak microcracking activity recorded by AE sensors.

## Observed AE Activity

The bulk of AE activity during the two years prior to the start of backfilling is concentrated close to the network of AE receivers (labeled A2 in Fig. 2), where the network has its best detection capabilities. Before the onset of backfilling, AE events observed above the target cavity are concentrated in two clusters labeled C1 and A1 in Figure 2. The linear

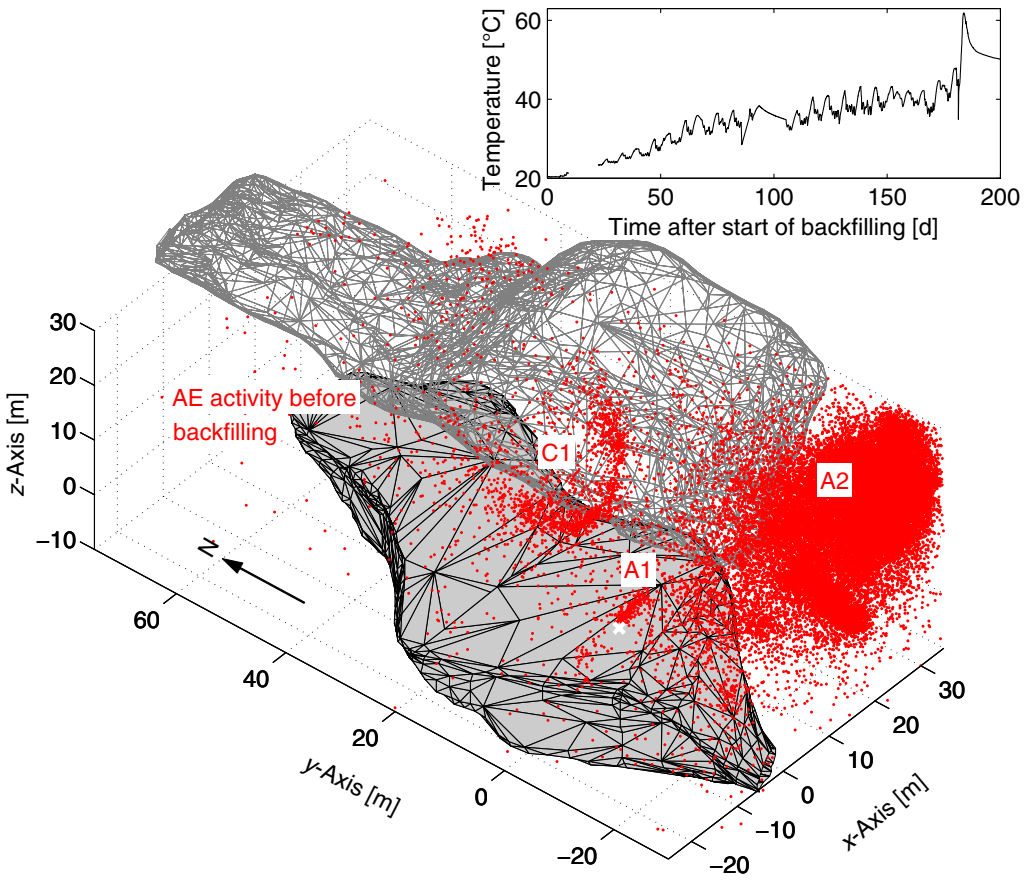


**Figure 2.** Located AE activity (dots) during the two years before the start of backfilling in the vicinity of the backfilled cavity. See Observed AE Activity section for explanation of C1, A1, and A2. The inset depicts the temperature profile recorded at the ceiling of the backfilled cavity (heavy white cross in main figure) during the backfilling process. The color version of this figure is available only in the electronic edition.

cluster of AE events close to the ceiling of the backfilled cavity (A1) is due to drilling activities in a borehole connecting the two depicted cavities. The other well-defined concentration of AE activity (C1) is at a distance of about 15–20 m above the cavity. This region is a curved zone of AE activity with a lateral extent of about 11 m and closely resembles similar patterns of AE clusters previously observed in the Morsleben mine. These structures, exhibiting steady microcracking activity at the same location and showing a circular shape (Spies and Eisenblätter, 2001), are suggested to be caused by inner, penny-shaped fractures at a significant distance from the nearest cavity. In one case, a fracture surface was identified at the cluster location by drilling a borehole (Spies and Eisenblätter, 2001). Apart from this event concentration, practically no microcracking activity is observed within the rock mass directly above the cavity during the two years preceding its backfilling.

After the onset of backfilling, AE activity in the region of cluster C1 strongly increases and a pronounced spatiotemporal migration of the microcracking activity can be observed (Fig. 3). Closer inspection of the event rate of cluster C1 indicates that it already showed a pronounced increase from a nearly steady state about 80 days before the start of backfilling (see inset of Fig. 3b). This activity increase coincided with drilling operations in the observation borehole (activity A1 in Fig. 2), suggesting a remote stress triggering. Immediately after the start of backfilling, AE locations in the vicinity of C1 are in agreement with those obtained before the start of backfilling (Fig. 4a). During later time intervals, however, activity on adjacent structures to the east increases whereas activity on C1 concentrates on its eastern part (Fig. 4b,c). This indicates a different spatiotemporal AE event evolution on the eastern and western parts of C1. Within the last weeks of backfilling, AE activity in the region is concentrated further to the east and activity on C1 nearly vanishes (Fig. 4d). The spatial orientation of C1 with respect to the cavities can be seen in Figure 5. The dip of the plane that best fits the AE event locations of C1 before the start and during the first 52 days of backfilling (Fig. 4a) is about 45°, with a strike direction of about S60°E. The orientation of best-fitting planes in this study was determined by visual inspection of the scatter of AE events around the possible planes projected into the data and additionally checked by plotting the AE events in a plane-centered coordinate system. The resolution of this method is on the order of 5°–10°.

AE activity on C1 before the start of backfilling is on the order of one event per day, and no event migration is resolv-

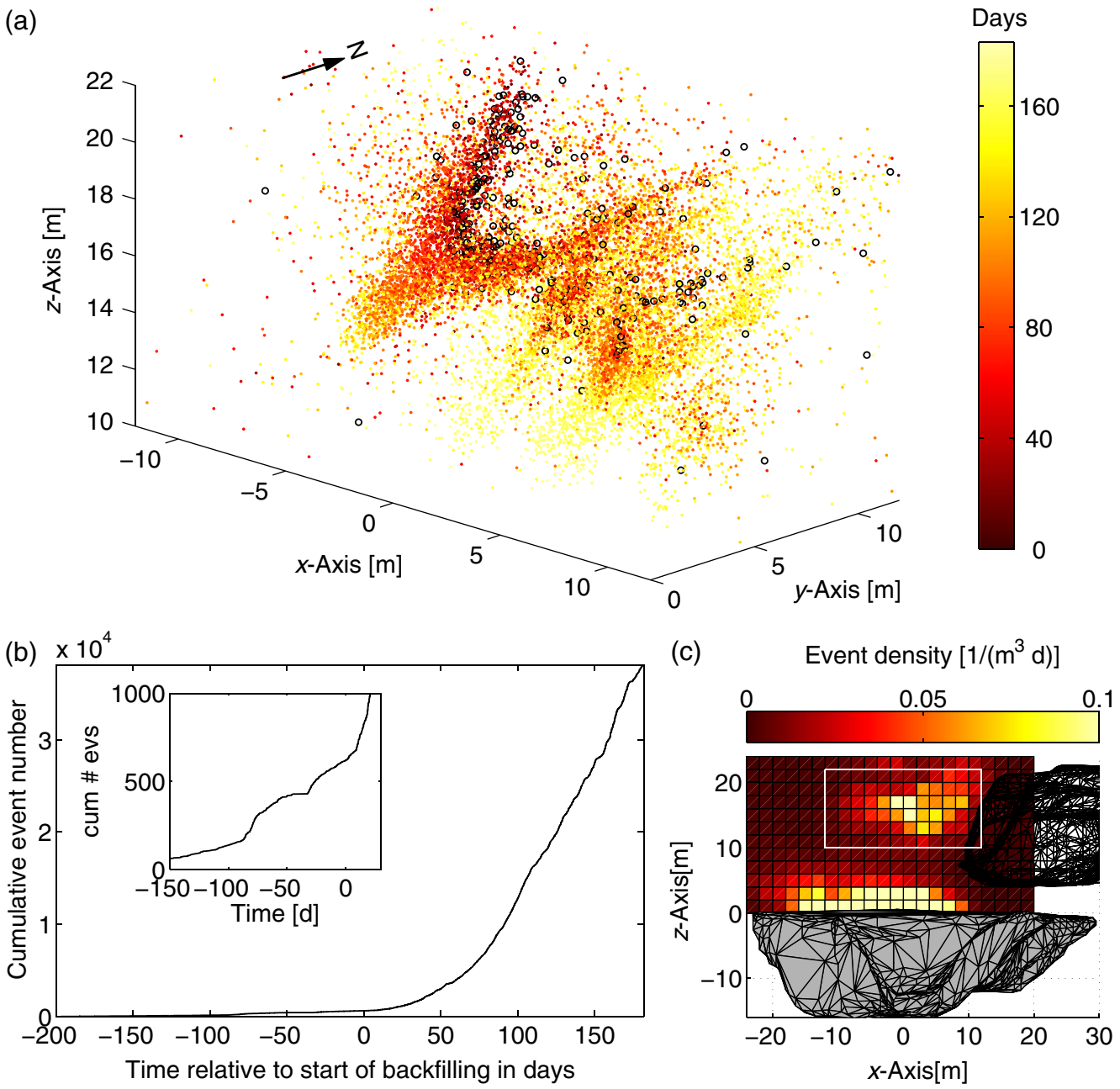


**Figure 3.** (a) AE activity with magnitudes ≥52 dB located within the vicinity of C1 (Fig. 2) before the onset of backfilling (open circles) and during the backfilling period (dots). The origin of the time axis corresponds to the beginning of backfilling. (b) Development of the cumulative number of AE events shown in (a). The inset in (b) shows a magnified look at the cumulative event number in the time interval 150 days before and 30 days after the start of backfilling. (c) The east–west cross section showing the event density above the backfilled cavity during the time of backfilling. The section is located at $y = 2$ and the extent of the cross-sectional volume is ±12 m; the white rectangle indicates the volume depicted in (a). The color version of this figure is available only in the electronic edition.

able. After the start of backfilling, however, a clear outward migration of the AE activity is observed (Figs. 3a, 5a,b, 6a,b), with different velocities in the northwestern and southeastern parts of C1 (subregions a and b of Fig. 6a, respectively). In contrast to the strong AE activity observed directly above the ceiling of the backfilled cavity, which shows a clear upward migration in accordance with the temporal evolution of the Coulomb stress field, the AE activity of C1 exhibits a downward migration toward the backfilled cavity (Fig. 6b). These two centers of activity seem to be separated by a distinct zone with very low microcracking activity, and no coalescence of the activity is observed during the backfilling process (spanning a total of 182 days; Fig. 6b).

Apart from the slow upward migration of AE activity immediately above the backfilled cavity, the supposed initiation of a new macrocrack (C2 in Fig. 5) at day 52 is observed.

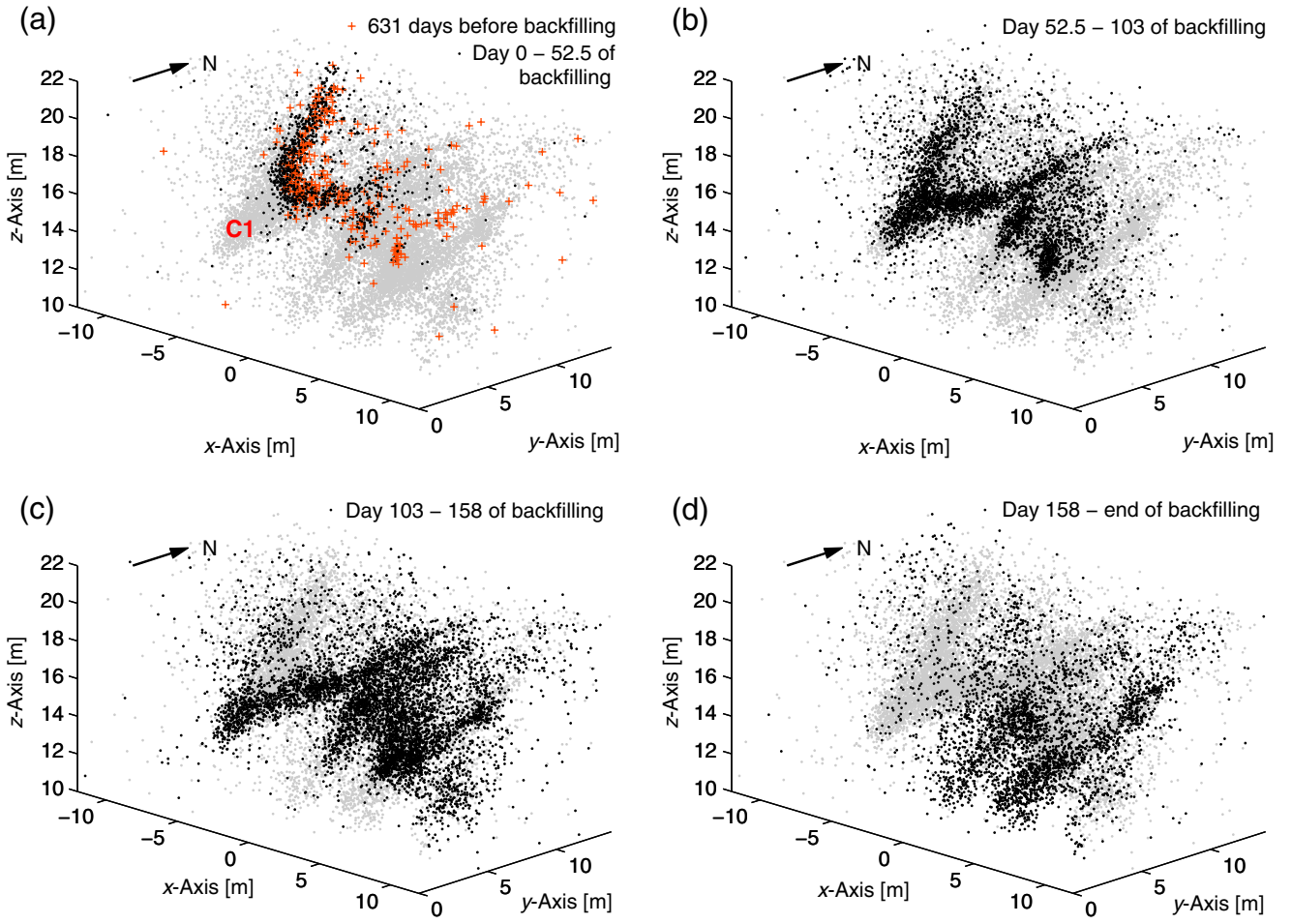


**Figure 4.** (a) AE activity with magnitudes ≥ 52 dB recorded from day 0 until 52.5 days after the start of backfilling (black dots). Also depicted is the AE activity recorded within the 631 days preceding the backfilling (crosses). AE activity during the entire 182-day backfilling period is indicated by gray dots and also depicted in (b–d). (b) AE activity from days 52.5 to 103 of backfilling. (c) AE activity from days 103 to 158 of backfilling. (d) AE activity from day 158 to the end of backfilling. The color version of this figure is available only in the electronic edition.

It is located directly above the backfilled cavity and finds its expression in a strong burst of AE activity up to a distance of nearly 10 m above the cavity at day 52 of backfilling (Fig. 6b; see also Becker *et al.*, 2010, for details regarding the identification of this macrocrack). The inferred best-fitting plane of this activity strikes N60°E, which is perpendicular to the left-hand cavity wall and the general strike direction of the folded salt body of the mine (Behlau and Mingerzahn, 2001) and has a dip angle of 35°. No spatiotemporal event migration is resolvable on C2, but a simultaneous activation of the entire active part is evident on day 52 (Fig. 5). Because of its location and AE pattern, C2 is termed a border fracture in this paper.

## Correlation of AE Activity with Calculated Stresses

### Stress Calculation

Stresses induced due to the backfilling process are calculated using a 2D plain strain FE thermoelastic model implemented with the commercial software ABAQUS (Dassault Systemes). Cavities within the 2D cross section are modeled as holes with boundaries that are free to move. Temperature boundary conditions inside the backfilled cavity are obtained from a vertical chain of temperature sensors with 0.5 m spacing and subhourly resolution, installed between the bottom and the ceiling of the cavity (Fig. 5a). Because gravity effects are not included in the modeling, it is assumed that stresses created during the formation of the cavities are already relaxed. Thus, only stress changes due to the thermoelastic effect of backfilling and due to the geometry of the cavities are studied. The vertical profile used in the stress modeling (black line in Fig. 5a) is oriented N60°E. All present geologic formations are modeled with the same material properties, and no structural interfaces between different geologic units are introduced in the model (see Becker *et al.*, 2010, for a detailed description of the stress modeling).

To study the response of the AE event distribution to stress changes, Coulomb stress changes (ΔCFS) are calculated from the results of the FE stress modeling according to

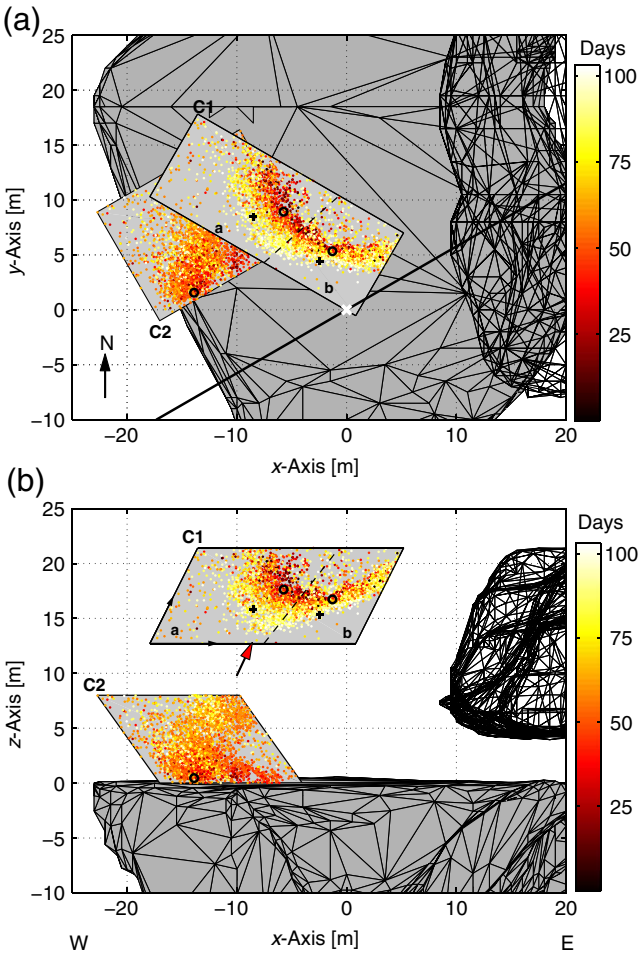


**Figure 5.** Orientation of clusters C1 and C2 (shown in light gray). Dots indicate the projections onto the respective plane of AE events recorded during the first 103 days of backfilling with magnitude ≥52 dB and within ±2 m of the assumed planes. Black circles and crosses on C1 and C2 indicate projections of the stress model node points used in Figures 7 and 8. The broken black line on C1 indicates the border between subregions a and b. (a) Map view with thick black line indicating the orientation of the 2D FE model. The heavy white cross indicates the location of the temperature sensor chain and the position of the vertical stress profile shown in Figure 6a. (b) East–west cross section. Black arrows at the edges of the C1 plane indicate origin and orientation of the along-strike and up-dip axes depicted in Figures 6a and 12b. The large arrow indicates the in-plane view direction onto C1 used in Figure 12a. The color version of this figure is available only in the electronic edition.

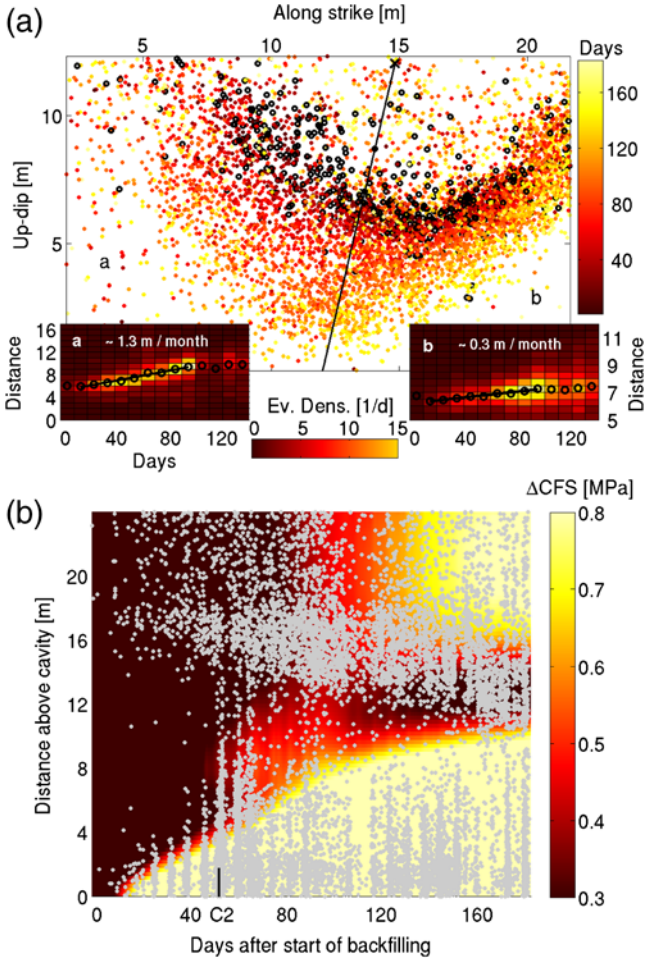


**Figure 6.** (a) The spatiotemporal AE event migration on inner fracture C1. AE events (magnitudes ≥52 dB) within ±2 m of the assumed surface are projected onto the C1 plane and color coded according to time (color scale to the right). Black circles indicate events occurring before the backfilling. The black line depicts the border between subregions a and b (northwestern and southeastern parts of C1, respectively), and the black cross at C indicates the assumed center of C1 activity. The insets quantify the spatiotemporal migration of AE activity away from center point C for subregions a and b. Depicted is the event density relative to center point C and the start of backfilling. Black circles indicate the average distance of AE events from C in the respective time period, and the black line is the linear fit between days 15 and 95. Migration velocities obtained by this fit are indicated in the insets. The color scale is saturated at 15 events/day. (b) Spatiotemporal development of maximum Coulomb stress changes for optimally oriented planes on a vertical profile above the backfilled cavity (heavy white cross in Fig. 5a). The AE activity with magnitudes ≥60 dB located above the backfilled cavity and projected onto the vertical profile is superposed. The tick mark at C2 indicates the occurrence of border fracture C2. The color version of this figure is available only in the electronic edition.

$$\Delta\mathrm{CFS} = \Delta\tau_r - \mu\Delta\sigma_n, \qquad (1)$$

in which $\Delta\tau_r$ is the change in shear stress on the plane in the expected slip direction, $\Delta\sigma_n$ is the change in normal stress with compression being positive, and $\mu$ is the effective coefficient of friction (Harris and Simpson, 1992). A value of 0.4 for $\mu$ is used in this study. The Coulomb failure concept states that failure is promoted when the Coulomb stress is increased and failure is suppressed when Coulomb stress decreases (e.g., Harris, 1998).

Coulomb stress changes of the 2D stress model have been projected onto the C1 and C2 planes, assuming constant stresses perpendicular to the strike of the stress model (Fig. 5). Stress histories for these node points are linearly interpolated to obtain Coulomb stress profiles with one sample per day from the higher resolution stress model output.

Spatially gridded Coulomb stresses on C1 or C2 presented in this study are calculated by spatially interpolating the projected stress model data at equally spaced grid points on the respective fracture plane.

Calculation of Coulomb stresses can either be performed for optimally oriented faults or for predefined failure mechanisms with specific strike, dip, and rake values. Because clusters C1 and C2 exhibit a planar structure, given strike, dip, and rake values are used for Coulomb stress calculation. Although strike and dip values can be taken directly from the orientations of C1 and C2 given above (Fig. 5), the rake value cannot be deduced from the AE event distribution. However, the pronounced increase of AE activity on C1 after the start of backfilling suggests an increase in Coulomb stress. In order to calculate Coulomb stress changes on C1, the rake value was varied between −180° and 175° in 5° increments while strike and dip values were held fixed. For C2, a rake value of 90° producing maximum Coulomb stress changes on this plane is assumed. The fact that no AE activity was observed prior to backfilling in the vicinity of C2 hints at an intact rock volume, and thus the orientation of the newly initiated macrocrack C2 should be governed by the thermal-induced stress field, which favors a rake angle of 90° on a plane striking N60°E in agreement with the orientation of C2.

## Results

In the absence of static stress changes leading to Omori-type event decay, the current seismicity rate scales with respect to a reference seismicity rate, such as the current stressing rate to the reference stressing rate (Dieterich, 1994). This approach assumes a steady state situation due to an only slowly varying stressing rate. In earthquake studies, which generally assume a Coulomb failure, the stressing rate is taken to be the Coulomb stressing rate or the shear stressing rate if the normal stress is assumed to be nearly constant (e.g., Dieterich, 1994).

Figure 7 shows the correlation between Coulomb stress rate and observed AE event rate for the inner fracture C1 and the border fracture C2. For the first 52 days of backfilling, a strong positive correlation between stress and event rate is observed for C1 and C2, which deteriorates thereafter. Although the calculated absolute stress changes and stressing rates on the inner fracture C1 are small (stressing rates in the order of a few kPa/day) compared to those observed close to the cavity (Fig. 7a,b), AE activity at C1 shows a pronounced increase after the onset of backfilling (Fig. 8a,b). This suggests a strong response to small stress changes due to backfilling activity. The strong positive correlation for C1 is observed for a wide range of different possible rake angles from −180° to −40° for the first 52 days of backfilling up to the initiation of border fracture C2 (Fig. 7c). These rake values indicate a component of normal faulting in the failure mechanism. For example, Figure 7c–f shows the daily Coulomb stress rates on subregions a and b of C1 for a rake value of −90°, leading to correlation coefficients ($r$) of 0.88 and 0.85 for the first 52 days of backfilling, respectively.

Apart from the first four days of backfilling, calculated Coulomb stress rates on C1 are always positive for the time interval studied in Figure 7, indicating a monotonously increasing absolute Coulomb stress. The stress rate curve for C1 also shows a cyclic behavior due to alternating periods of thermal expansion and contraction of the rock mass close to the ceiling of the cavity caused by the alternation of periods with increasing and decreasing temperatures (Fig. 2). For the position on C1 studied in Figure 7c, the FE calculation indicates a temperature change of only 0.03° C for the first 100 days of backfilling due to the slow propagation of the thermal front, whereas temperature fluctuations at the ceiling of the backfilled cavity are on the order of up to 2–3° C per day around day 50 (Fig. 2). A temperature increase at the cavity ceiling corresponds to a maximum of the Coulomb stress rate at C1, whereas a temperature decrease coincides with a minimum of the calculated stress rate at C1. At the ceiling of the cavity in the vicinity of C2, the temperature fluctuations lead to periods with decreasing absolute Coulomb stresses, that is, Coulomb stress rates $< 0$ without AE activity (Fig. 7a).

After day 52, which coincides with the initiation of macrocrack C2, the correlation between observed event rate and calculated Coulomb stress rate is either less pronounced ($r = 0.65$ for subregion a on C1, Fig. 7c,d) or nonexistent ($r = 0.07$ for subregion b on C1, Fig. 7e,f). This is also true for rake values other than −90° (Fig. 7c inset). A slight general increase of the correlation coefficient with increasing rake value is observed in the interval from −180° to −40°. The generally much lower correlation coefficients after day 52 suggest an influence from processes not accounted for by the 2D FE model, such as static stress changes due to macrocrack activity or processes like creep or cataclastic deformation. However, a modification of the original strike and dip values of C1 also has the potential to cause this worse fit.

Subregions a and b of C1 demonstrate a strikingly different behavior after day 52. Although AE event rates on subregion a still follow the general pattern of the calculated Coulomb stress rates, AE activity on subregion b is clearly at odds with the stress rate curve, exhibiting pronounced event rate maxima during stress rate minima after day 65 of backfilling. Subregion b also exhibits an overall gradual increase of the event rate maxima up to day 102, when the calculated Coulomb stress rates and AE activity on subregion a are already decreasing. This might indicate a change in faulting style on subregion b after day 65. This change could be linked to the general eastward migration of AE activity in the vicinity of C1 and the activation of new structures possibly modifying the stress field (Fig. 4). The temporally increasing influence of a nearby cavity to the east on the stress field, also evident in the stress profile of Figure 6b (upper right corner), might influence this event migration. However, due to the complex pattern of AE activity during later times of backfilling, it is difficult to identify individual planes in the event distribution. Another noteworthy observation is the extremely low number of events observed directly after the initiation of C2 in the vicinity of C1 (Fig. 7c,e).

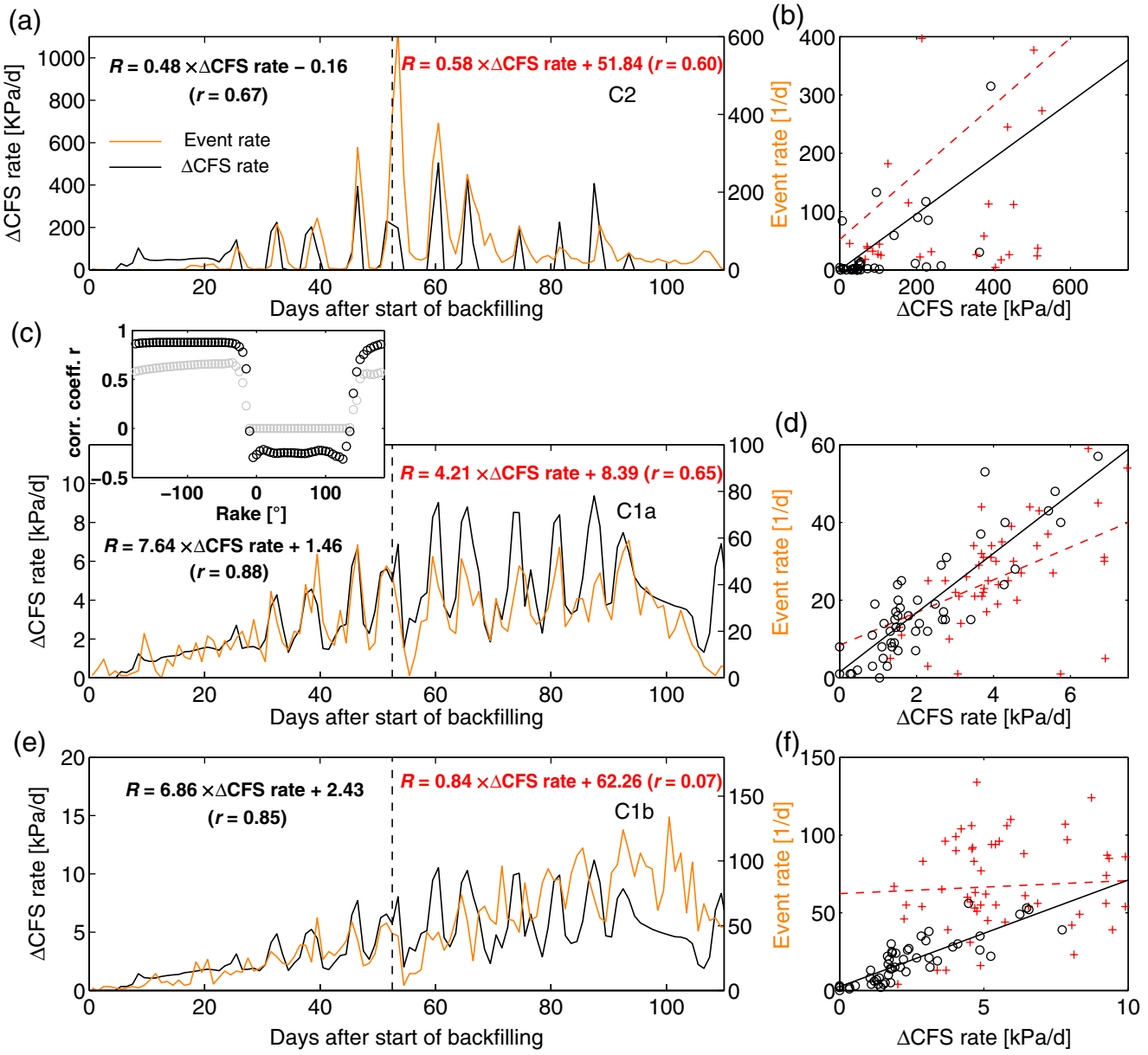


**Figure 7.** (a) Correlation between Coulomb stress rate calculated for a rake value of 90° and event rate for C2. Events are taken from within ±2 m of the surface shown in Figure 5. Only positive Coulomb stress rates during the time intervals of the new absolute Coulomb stress maxima are presented in the stress rate curve. (b) The daily event rate over daily Coulomb stress rate for C2 for days 1–52 (circles) and days 53–110 (crosses). (c)–(f) Corresponding presentations for subregion a of C1 (c, d) and subregion b of C1 (e, f) for an assumed rake of −90°. The inset in (c) shows the correlation coefficient $r$ depending on the rake value for subregion a of C1 for days 1–52 (black) and days 53–110 (gray). The stress model node points used for calculations are depicted by black circles in Figure 5a. The vertical dashed line in (a), (c), and (e) indicates the supposed initiation of border fracture C2. The solid and broken lines in (b), (d), and (f) indicate the best-fitting trend of a linear regression analysis for days 1–52 and days 53–110, respectively. The numerical values of this analysis and the correlation coefficient $r$ are given in the corresponding plots (a), (c), and (e) in the respective time interval. The color version of this figure is available only in the electronic edition.

For C2, a generally weaker correlation between Coulomb stress rate and event rate is observed ($r = 0.67$ for days 1–52 of backfilling and $r = 0.60$ for days 53–110 of backfilling, Fig. 7a,b) than for subregion a of C1. This observation might be explained as follows (see also Fig. 7a): (1) for the first 16 days of backfilling, only two events were recorded, although significant positive Coulomb stress rates were calculated for C2; (2) the initiation of the border fracture on day 52 resulted in an exceptionally large number of AE events; and (3) tensile stresses occurred close to the ceiling of the cavity during the rapid cooling of the rock mass during times of negative Coulomb stress rates, inducing microcracking (e.g., around day 70, Becker *et al.*, 2010). For Figure 7a,b, negative Coulomb stress rates were set equal

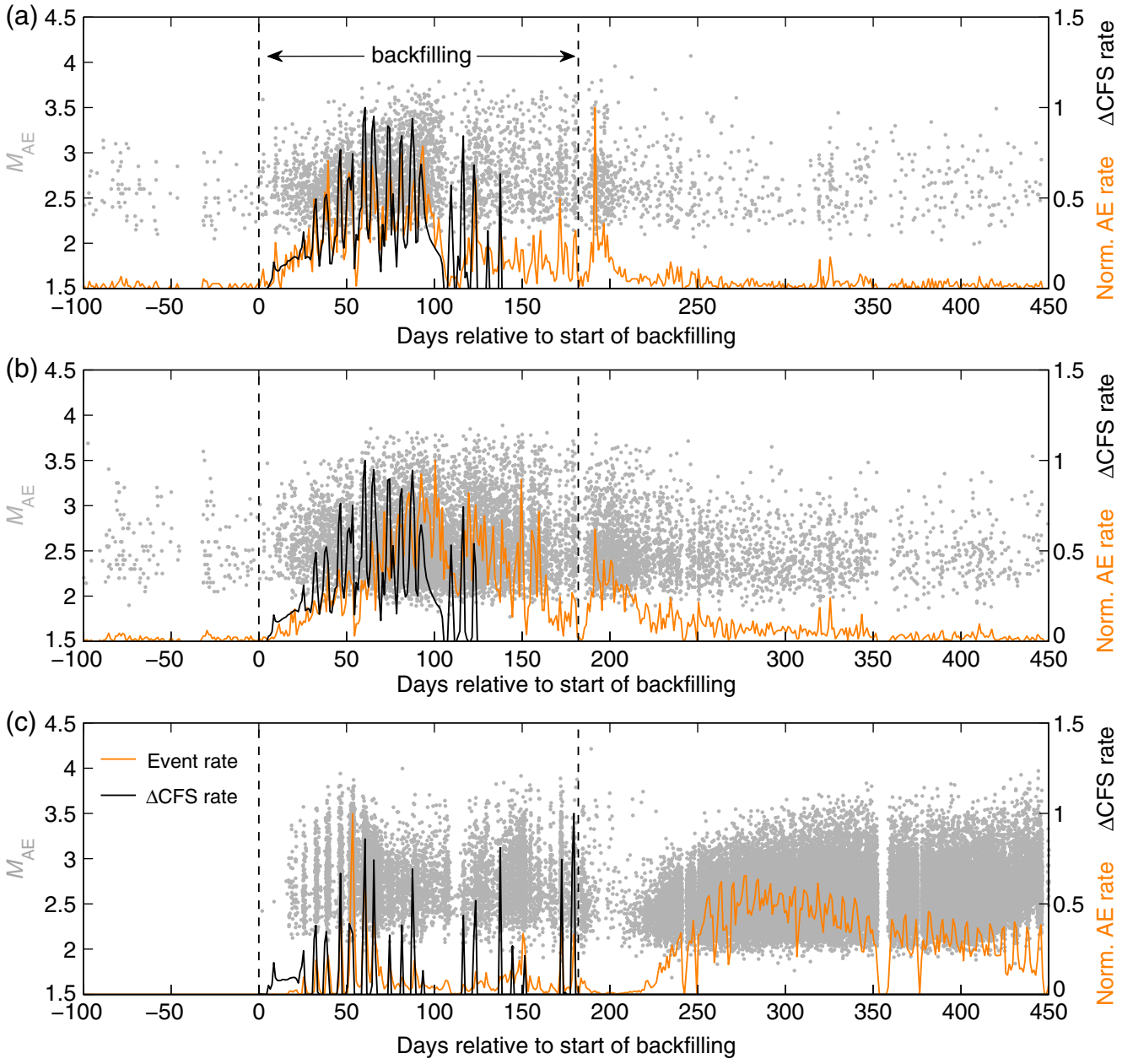


**Figure 8.** Long-term comparison between observed AE activity within ±2 m of the assumed plane of the respective cluster and Coulomb stress rates for (a) subregion a and (b) subregion b of C1, as well as for (c) the border fracture C2. Gray dots indicate the magnitude over time evolution of AE activity in the respective volume. Event rates and Coulomb stress changes (solid lines, see [c] for legend) are normalized with respect to their maximum. Stress rates for the C1 subregions are calculated for the respective node points depicted in Figure 5 by the black crosses, assuming a rake value of −90°. For C2 the same node point as in Figure 7a was used, assuming a rake value of 90°. The color version of this figure is available only in the electronic edition.

to zero because $\Delta CFS < 0$ should inhibit shear microcracking.

Enlarging the study period to 100 days before the start and about 270 days after the stop of backfilling shows that steady, low-level microcracking activity associated with C1 also occurred before the start of backfilling activity (Fig. 8a,b). In contrast, the newly created border fracture C2 showed no microcracking activity before the onset of backfilling and, apart from two single events, also no recordable microcracking processes up to day 16 of backfilling (Fig. 8c), although thermal-induced stresses at its location were considerably higher than at C1 and reached values of up to 3 MPa at day 52 of backfilling.

In Figure 9, spatially resolving Coulomb stress changes on C1 indicates that the entire plane on which AE activity is located experiences positive Coulomb stress changes, and the regions on C1 exhibiting AE activity during the first 52 days of backfilling show comparable absolute stress changes. This is

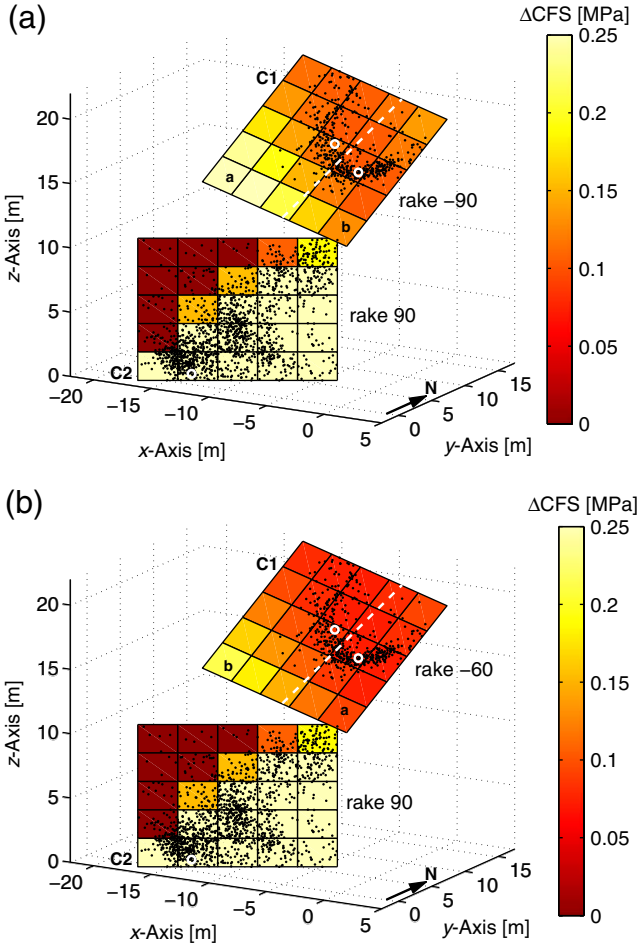


**Figure 9.** (a) The Coulomb stress change on C1 for a rake value of −90°. (b) The Coulomb stress change on C1 for a rake value of −60°. For C2, a rake value of 90° is assumed in (a) and (b). Stress changes for day 52.8, corresponding roughly to the moment of C2 initiation, are depicted. AE activity within ±2 m of C1 and C2 is projected onto the respective plane (black dots). For C2, all AE activity recorded for days 52.75–53.95 and days 58.75–61.2; the presumed initiation and reactivation of this macrocrack is shown. The depicted AE activity of C1 belongs to the time intervals of days 43.75–46.25 and days 49.25–52.75, corresponding to the last two stress loading phases before C2 initiation. The broken white line on C1 indicates the border between subregions a and b. White circles indicate the projection of stress model node points used for stress calculation in Figure 7. The color version of this figure is available only in the electronic edition.

in agreement with the observed AE activity on C1 for the beginning of backfilling, showing an enhanced activity over the entire active area. However, a somewhat larger stress increase is observed in areas of C1 that show no AE activity. The fact that no AE activity was observed in this higher stress area might suggest that the controlling factor in AE activity is the current location of the outward-expanding AE event cloud on C1. In contrast, Coulomb stresses calculated for C2 indicate a curved boundary between a region with high stress increase and a region above with much smaller Coulomb stress increase (Fig. 9). This corresponds to the AE activity during the initiation and reactivation of C2, which is almost exclusively confined to areas with a calculated Coulomb stress increase in excess of 0.25 MPa. These observations support the choice of the rake value for C2. The most likely nucleation point for C2 is at the ceiling of the backfilled cavity, where the Coulomb stress reaches its maximum and a large concentration of AE events is observed (Fig. 9).

As evident from Figure 7c,e, the initiation of C2 temporally coincides with a clear change in the pattern of AE activity on C1. This change might be either caused directly by C2 or other underlying processes. A possible explanation in conjunction with C2 is the static stress changes due to a dislocation on C2. These stress changes can be qualitatively estimated using the Okada solutions for dislocation on a fault in a homogeneous half-space (Okada, 1992), an approach routinely followed to calculate, for example, static stress transfer from one earthquake fault to another (King *et al.*, 1994; Freed, 2005). For this study, we adapted some of the COULOMB 3.1 software routines (Lin and Stein, 2004; Toda *et al.*, 2005) using the Okada solutions to our problem and calculated the Coulomb stress changes on C1 resulting from a dislocation on C2 (see Fig. 10 for fault geometry). For C2 a rake value of 90° was used, and for C1 all rake values exhibiting a correlation coefficient $\geq 0.86$ on subregion a of C1 for the first 52 days of backfilling were considered. We arbitrarily chose a dislocation on C2 of 1 mm. Larger or smaller slip magnitudes only change the amplitude of the resulting stress changes but preserve the general stress change pattern.

Calculated Coulomb stress changes (Fig. 10) indicate a decrease in Coulomb stress for the parts of subregion b of C1 active before initiation of C2, which is in agreement with the low event rates observed in that region immediately after the initiation of C2 (Fig. 7e). For subregion a, the result is more sensitive to the assumed rake value. For example, for a value of −90°, a Coulomb stress increase for the entire area is observed (Fig. 10a), whereas a rake value of −60° results in a stress decrease in areas showing especially strong AE activity immediately before the initiation of C2 (Fig. 10b). This can qualitatively explain the low event rates in subregion a of C1 directly after the initiation of C2 (Fig 7c). The same is also true for rake values between −60° and −40° (Ⓔ see Fig. S1, available in the electronic supplement to this article). Together with the slightly higher correlation coefficients for rake values between −40° and −60° for the time interval from days 53–110 (Fig. 7c inset), this might suggest a rake angle in the −40° to −60° range. However, no significantly different AE behavior for regions with calculated Coulomb stress increase and decrease on subregion a of C1 can be observed after initiation of C2.

## Discussion

### Location Accuracy and Completeness of the AE Catalog

Although there is a possible shift in the absolute locations of recorded AE events due to errors in the homogeneous

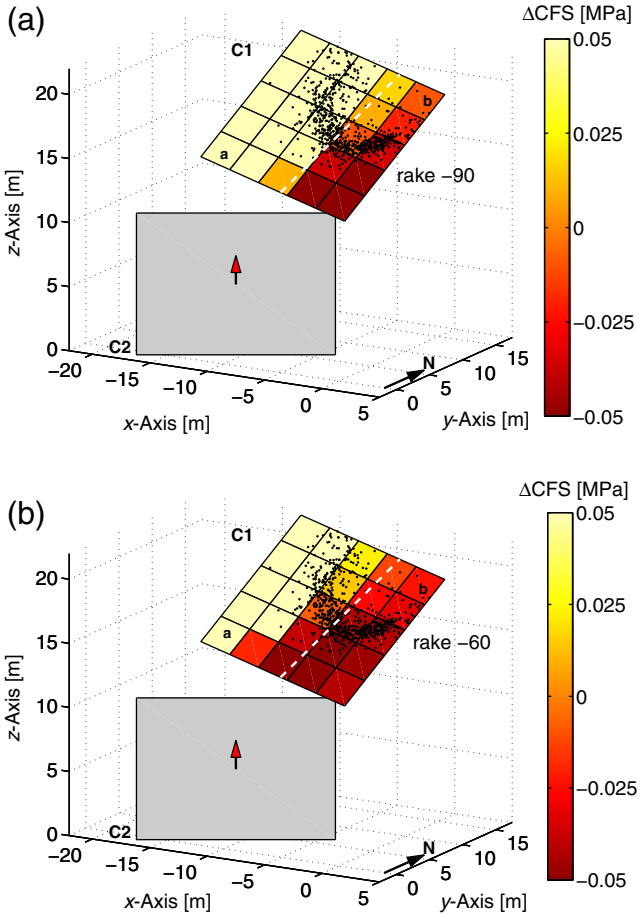


**Figure 10.** Static Coulomb stress changes calculated for C1, assuming displacement on C2. (a) The Coulomb stress change on C1 for a rake value of −90°. (b) The Coulomb stress change on C1 for a rake value of −60°. The assumed slip direction of C2 (rake of 90°) is indicated by the arrow. The dashed white line on C1 indicates the border between a and b. The dots on C1 indicate AE events located within ±2 m of C1 during days 42.75–52.75 of backfilling, and therefore indicate the approximate location of microcracking activity on C1 at C2 initiation. The color version of this figure is available only in the electronic edition.

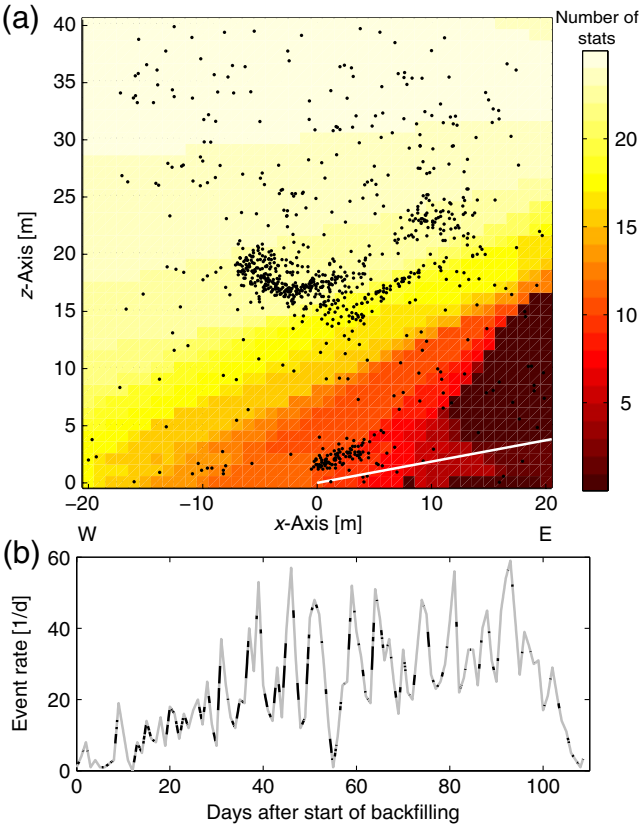


**Figure 11.** (a) The color-coded grid indicates the number of AE receivers reached from the respective grid point with a straight line without hitting a cavity. For regions with only a few direct ray paths, large travel-time residuals prevent an event location. The depicted east–west cross section is calculated at $y = 0$. AE activity with magnitudes ≥48 dB during the 631 days before the start of backfilling and occurring in the range $-2$ m $\leq y \leq 14$ m is projected onto the cross section (black dots). The white line indicates the projection of a borehole. (b) Daily event rate on subregion a of inner fracture C1. The gray portions indicate time intervals with an AE event catalog identified as complete, and the black portions indicate incomplete time intervals. The completeness analysis has an hourly resolution, whereas the event rate curve is constructed from one sample per day. The color version of this figure is available only in the electronic edition.

velocity model used for localization, which is also seen in other studies (e.g., Naoi *et al.*, 2011), the relative event location between events belonging to the same structure is probably more reliable. This can be seen in Figure 11a, in which AE activity linked to working activity in a borehole is vertically offset by about 1–2 m from its true location at the western end of the borehole. However, events show a tight clustering following the orientation of the borehole, thus indicating a high relative accuracy, and events associated with the inner fracture are confined to a narrow plane of activity (Fig. 12a). This indicates that the relative location accuracy for closely spaced events is high enough to detect an event migration of less than 1 m/month during the observation period (Fig. 12b–d). A former study of this dataset (Becker *et al.*, 2010) found a location uncertainty of about 1 m for events in the area of C2 and no large systematic location errors. However, the location accuracy is spatially variable due to the different receiver configurations reached by direct ray paths from different places.

Because of shadowing effects by nearby cavities, the event catalog in the mining environment is often incomplete. The absence of recorded AE activity in the eastern part of the borehole in Figure 11 is probably such a case. The position up to where AE events linked to the borehole are recorded correlates well with the region in which at least eight direct ray paths to receivers are observed. In the first location attempt using only *P* waves, these eight *P* arrivals are necessary for an accepted event location. The region between 8 and 12 m above the backfilled cavity has at least as many direct ray paths to receivers as the western termination of the borehole where AE events are recorded. This suggests that the observed gap in AE events in this region above the cavity

(Figs. 3c and 6b) is real and not due to a shadowing effect from nearby cavities. The same is true for the region above C1, which is also well covered by direct ray paths but shows no AE activity. Thus, the semicircular shape of the inner fracture seems to be a real feature and not an artifact.

Apart from the spatial completeness, the temporal catalog completeness may also vary. Because the studied activity is concentrated in a small area and no changes to the geometry of the recording network or the data analysis were performed, the overall magnitude of completeness of the investigated AE catalog should not change with time. However, working noise in the mining environment may cause an incomplete event registration. Using an earlier developed method to identify incomplete time periods with hourly resolution in the studied dataset (Becker *et al.*, 2010) indicates that during the first 110 days of backfilling, the event catalog is complete for 82% of the recording time (Fig. 11b). Correcting for incomplete time intervals by taking the average hourly event rate from the complete time intervals of one day as constant for the whole day results in the relation $R = 8.05\Delta\mathrm{CFS} + 3.03$, with a correlation coefficient $r$ of 0.86 for the first 52 days of backfilling for subregion a of C1 and a rake value of −90°. This is comparable to the results in Figure 7c without correction for possible catalog incompleteness. This suggests a minor influence of the catalog incompleteness for this investigation. Using an AE event catalog with hourly resolution and interpolating the incomplete time intervals or concentrating only on the complete hours is not feasible due to the low daily event rates in the vicinity of C1 (Fig. 7c,e).

### Assumptions in the Coulomb Stress Calculations

Projecting stress model results on C1 and C2 (Figs. 7–10) assumes that the stress field is constant perpendicular to the strike direction of the 2D model. Although this is certainly not the case for regions at larger distances from the stress profile because the cavities incorporated in the stress model have finite lengths and variable cross sections perpendicular to the strike of the stress model, the investigated AE events in this study are close enough to the stress profile (Fig. 5) that such an approach seems justified. Furthermore, the stress model is oriented perpendicular to the strike direction of the walls of the backfilled cavity as well as to the general strike direction of the geologic units of the mining complex, resulting in a geometry and lithology rather constantly perpendicular to the stress profile. However, simplifications due to the 2D character of the stress model still remain.

Another concern regarding the temporal analysis of Coulomb stresses (Figs. 7, 8) might be the use of representative stress histories at specific points for extended areas when stresses and stress rates in fact show some variability on the investigated plane (see Fig. 9). However, as seen in Figure 12c,d, the majority of the observed AE activity is concentrated in a rather narrow, migrating AE front and not spread out over the entire plane of C1. When we compare the stress rate curves for representative points on subregions a and b for the first 110 days of backfilling (Figs. 7c,e), it is apparent that they are very similar. This general similarity is also observed for node points further down on C1 (Fig. 8a,b) that correspond to later positions of the migrating event front. All these stress rate curves exhibit a generally similar behavior during the beginning of backfilling and hint at spatially smooth Coulomb stress changes for a mechanism favoring AE activity on C1.

Because of the purely elastic formulation used in the stress modeling, processes like the formation of new fractures and macrocracks, creep, or cataclastic deformation are not accounted for. The high-stress transients induced during backfilling, as well as the significant temperature increase close to the backfilled cavity, facilitate such failure processes. A growing discrepancy between calculated and actual *in situ* stresses can thus be expected and may partly explain the lower correlation coefficients between observed event and calculated stress rate for later times. For the initiation of border fracture C2, which temporally coincides with a clear deterioration in the correlation between observed AE event rates and calculated Coulomb stress rates on C1 (Fig. 7c–f), we tried to estimate the static stress changes due to such an inelastic deformation.

The fact that the calculated static Coulomb stress changes can only partly explain the AE pattern on the inner fracture C1 after the initiation of the border fracture C2 can have several explanations. One of them might be incorrect strike, dip, and rake values chosen for C2; however, because C2 seems to be a macrocrack in intact rock, the mechanism of C2 probably obeys the acting stress field as observed for other assumed Coulomb failure events in the mining environment (e.g., Naoi *et al.*, 2011). The plane best describing the distribution of AE activity of C2 is in good agreement with the optimally oriented plane as obtained from the FE model. Furthermore, regions with high AE activity during the initiation and reactivation of C2 correlate well with areas of high positive Coulomb stress changes on that surface (Fig. 9), supporting a rake value of about 90° for C2. Slight changes in this rake value do not significantly change the result of Figure 10. A completely different mechanism is not likely, because the free surface of the cavity demands a vertical stress equal to zero at the supposed initiation point of C2 and the distribution of AE activity fixes the approximate strike and dip values of C2. Limiting the rupture area of C2 only to regions exhibiting high AE activity during its initiation (Fig. 9) also does not significantly change the stress change pattern in Figure 10.

A more severe problem might be the assumption of the Okada formulation that the dislocation takes place in an elastic, homogeneous half-space. The fact that the border fracture initiates at the top of a cavity, as well as the presence of further cavities, modifies the resulting stress field and may be one explanation for the misfit between modeled stress changes and observed AE history. The stress modeling results in this study seem to indicate that a purely thermoelastic FE

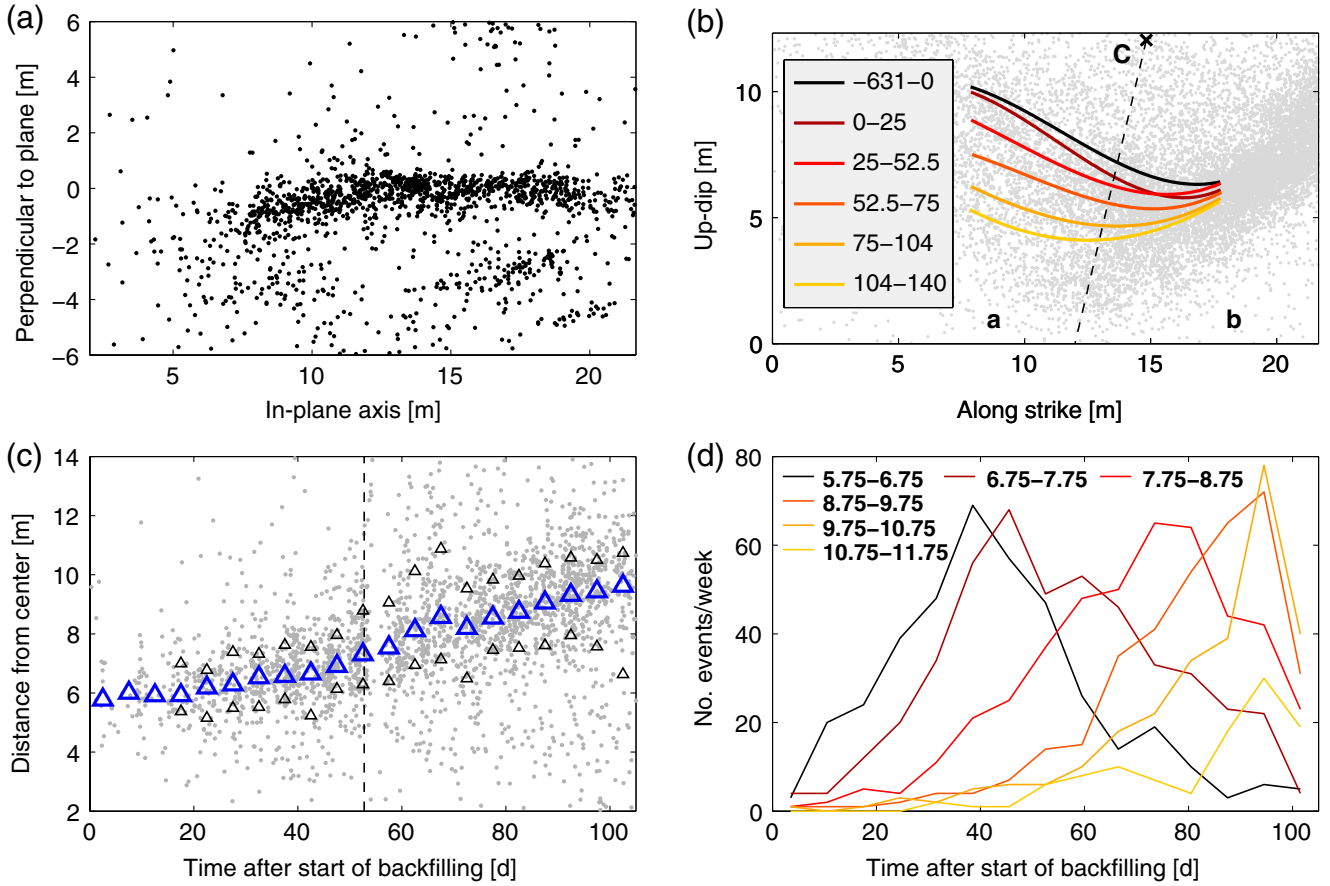


**Figure 12.** (a) In-plane view of AE activity (magnitudes ≥52 dB) up to day 52.75 associated with C1. The view direction is indicated in Figure 5b by the arrow. (b) Isochrones of spatiotemporal AE event migration on C1. Color-coded lines indicate the spline interpolation through all AE activity observed within ±2 m of C1 during the time intervals given in the color legend, indicating the average position of AE activity. The black cross labeled C indicates the assumed center of AE activity on C1, the broken black line is the border between subregions a and b, and gray dots indicate AE events with magnitudes ≥52 dB occurring within ±2 m of C1. (c) Higher resolution version of inset a in Figure 6a. The gray dots indicate the distance of events in subregion a of C1 with respect to the assumed center of activity indicated in (b). Large triangles indicate the median distance of events in consecutive five-day intervals, and small triangles indicate the 20th and 80th percentile for time intervals with more than 50 events. The vertical broken line indicates the moment of C2 initiation. (d) The weekly event count for different distance ranges from center C of C1 using the data depicted in (c). The time-delayed increase of AE activity for different distance ranges and the subsequent decrease is indicating the passage of a migrating AE front. The color version of this figure is available only in the electronic edition.

stress modeling incorporating both the cavity geometry and the temperature history is able to estimate the true stress field reasonably well as long as no inelastic processes like fracture initiation or creep are taking place. To calculate stress changes due to inelastic deformations, the incorporation of the cavity geometry or a test for creep or the cataclastic deformation often observed in more ductile materials (Scholz, 2002) seems necessary.

## Character of Observed Macroscopic Failure Processes

The present study investigates the spatiotemporal behavior and correlation with induced stresses of two concentrations of microcracking activity in an abandoned salt mine. We interpret them to be spatially distinct macroscopic failure processes exhibiting clearly dissimilar characteristics.

The inner fracture C1 is a planar (Fig. 12a), pre-existing structure at considerable distance from the next cavity where a spatiotemporal event migration is observed. Although no event migration on C1 is resolvable for the time before backfilling, a clear migration with higher velocities on subregion a than b of C1 can be recognized immediately after its start (Fig. 12b). A careful analysis of the event evolution reveals that for the time up to the initiation of C2 on day 52, a migration of the AE events is resolvable (Fig. 12b,c). Apart from the outward migration of the mean position of AE activity (Fig. 12b), it is apparent from Figure 12c,d that the outward expanding event front is trailed by a kind of back front, behind which the AE activity decreases once again. Effectively, this results in a narrow, outward-migrating zone of active microcracking. This zone seems to represent the current position of the highest stress concentrations, whereas regions

behind this active zone seem to have released some stress due to their earlier AE activity. The immediate response of this narrow zone to the small thermal-induced stress changes indicates that it is in a critical state and small stress perturbations can induce microcracking. This observation of an immediate AE response to thermal stressing was also made in heating experiments in hard rock laboratories (e.g., Falls and Young, 1998; Andersson *et al.*, 2009). In contrast to those studies, in which the AE activity was located in borehole breakout notches within the first meter of the damaged granite without substantial event migration, we observe a migrating, planar front of AE activity at a distance of about 15 m from the cavity in a much softer material.

Causes for such a migrating AE front could be an outward-expanding excavation damage zone (e.g., Young and Collins, 1999), the response of the rock mass to a slowly migrating temperature anomaly (e.g., Becker *et al.*, 2010), a migrating pore pressure perturbation (e.g., Moriya *et al.*, 2006), or microcracking activity occurring in the crack tip damage zone of a slowly growing fracture in intact rock (e.g., Schultz, 2000; Scholz, 2002) or on a reactivated rupture surface or structural interface (Spies and Eisenblätter, 2001). The observed AE activity (Fig. 12) suggests microcracking activity in a planar, rather narrow, zone of stress concentration. Such a behavior resembles the subcritical growth of a fracture with propagation velocities orders of magnitude below those of a dynamic fracture (e.g., Schultz, 2000; Scholz, 2002). This slow crack growth can continue for an extended period of time as long as the crack does not enter the region of unstable equilibrium where an unlimited crack growth is initiated (Scholz, 2002). The maximum propagation velocity of about 1 m/month for the front of AE events is within the range of crack growth velocities observed in the laboratory ($1 \times 10^{-9}$ and $1 \times 10^{-3}$ $ms^{-1}$; Atkinson, 1984). The presence of a highly complex geology in the study region, as well as the earlier observation of a circular cluster of AE activity showing a spatiotemporal outward expansion that was confirmed as a growing fracture at the interface between rock salt and anhydrite by two boreholes (Spies and Eisenblätter, 2001), might point to a process between geologic boundaries or on a reactivated rupture surface. This would be comparable to the activation of shear fractures at a larger distance from the active excavation (which have the potential to release larger amount of stored stresses), resulting in larger magnitude events in case of failure (e.g., Richardson and Jordan, 2002).

The different behaviors observed for subregions a and b of the inner fracture might be partly governed by the presence of a second cavity above the backfilled one (shown in black outline in Fig. 5), thereby influencing the background stress field. This one is much closer to subregion b of C1 than to subregion a and exhibits a strong influence on the observed maximum Coulomb stress change on optimally oriented planes during later times of backfilling (Fig. 6b). This larger scale stress concentration is possibly also responsible for the general eastward migration of AE activity in the vicinity of C1 with time (Fig. 4). Stresses created due to the presence of the cavity might be high enough to initiate AE activity, obeying a new failure mechanism in subregion b, whereas subregion a at a larger distance from the cavity (Fig. 5) still favors the original mechanism of C1.

In contrast, the border fracture C2 shows no discernible event migration (Fig. 5). The instantaneous occurrence of AE activity over an extended region on day 52 of backfilling and the absence of AE events before and during the beginning of backfilling (Fig. 8c), despite the presence of significantly higher Coulomb stress changes than at the inner fracture, indicates a dynamic macrocrack formation in formerly intact rock. Such a failure mechanism is also characteristic for rockburst events being induced around active excavations due to the high stress changes within the first few meters of the rock mass (e.g., Gibowicz and Kijko, 1994; Richardson and Jordan, 2002).

## Conclusions

The spatiotemporal pattern of AE activity before and during backfilling and its correlation with calculated Coulomb stress changes leads to the following four conclusions.

The increase of AE rates and the outward migration of a rather narrow tip zone of AE activity of a semicircular structure at a significant distance (15 m) from the source region of the thermal stresses was instantaneously triggered at the start of backfilling. The human-induced absolute Coulomb stress increase at this inner fracture was only about 100 kPa during the first 50 days of backfilling, and stress changes of a few kPa already led to a pronounced increase of AE activity. This indicates that the inner fracture was in a critical state before the beginning of backfilling operations. The analysis of AE activity several months before the backfilling operation supports this interpretation, because the semicircular zone is already clearly recognizable in this time interval.

The outward migration of this semicircular zone of AE activity is directed toward the border of the backfilled gallery, with migration velocities reaching values up to 1 m/month, depending on the azimuth. The overall shape and migration clearly suggest the existence of a macrofracture with a diameter of more than 10 m. Such a fractured patch on a pre-existing fault, which is aseismically growing, is an important but rarely observed process. It can give insights into the nucleation process of catastrophic failure events, such as the earthquake nucleation process. Our study quantifies the size of the nucleation fracture and its growth velocity. We find varying growth velocities in different azimuthal directions, which do not correlate with the azimuthal pattern of the triggering stresses. This indicates that the growth velocity is likely controlled by the pre-existing stress field and not by the induced stress field.

The induced border fracture occurred with a significant delay to the beginning of backfilling activity. The calculated increase of local Coulomb stress at the supposed initiation

point at the time of occurrence was about 3 MPa. This indicates that the volume was not in a critical state before the beginning of backfilling operations. The border fracture was thus most likely fully induced by the human-induced thermal stresses. Furthermore, the absence of a resolvable AE event migration linked to this border fracture indicates a fast rupture process, such as in an earthquake or rock burst event.

The modeled temporal pattern and the magnitudes of thermoelastic Coulomb stress changes correlate well with the general pattern and the rates of induced AEs during the first 52 days of backfilling. We find a sudden breakdown of this high correlation coincident with the occurrence of the border fracture. This indicates that the development of induced macrofractures or other inelastic processes introduce stress heterogeneity sufficiently large to control the occurrence of smaller events at a later stage of human activity. The AE activity is thus more difficult to predict if the operations last longer. However, the combination of stress modeling and seismicity monitoring is a promising tool to better reveal such 3D stress heterogeneity in mining environments. For instance, the monitoring of small events can be used to detect and study the occurrence of larger aseismic slip events or the development of a cataclastic zone.

## Data and Resources

The acoustic emission (AE) event database and information concerning the recording system and the geometry of the underground cavities were provided by the Bundesanstalt für Geowissenschaften und Rohstoffe (BGR, the Federal Institute for Geosciences and Natural Resources). The BGR operates the array on behalf of Bundesamt für Strahlenschutz (BfS, the German Federal Office for Radiation Protection). Information about the backfilling process (e.g., temperature profiles used in the stress modeling) was provided by Deutsche Gesellschaft für den Betrieb von Endlagern (DBE). Currently, the AE event database and the temperature profiles are not released to the public.

## Acknowledgments

We thank David Collins, Cezar Trifu, and an anonymous reviewer for helpful comments and constructive suggestions to improve the manuscript. This research was funded by Deutsche Forschungsgemeinschaft (DFG) through Grants BE 4602/1-1 to D.B. and CA 459/2-1 to B.C.

## References

Andersson, J., and C. Martin (2009). The Äspö Pillar stability experiment: Part I - Experiment design, *Int. J. Rock Mech. Min. Sci.* **46,** 865–878.

Andersson, J., C. Martin, and H. Stille (2009). The Äspö Pillar stability experiment: Part II - Rock mass response to coupled excavation-induced and thermal-induced stresses, *Int. J. Rock Mech. Min. Sci.* **46,** 879–895.

Atkinson, B. (1984). Subcritical crack growth in geological materials, *J. Geophys. Res.* **89,** 4077–4114, doi: 10.1029/JB089iB06p04077.

Becker, D., B. Cailleau, T. Dahm, S. Shapiro, and D. Kaiser (2010). Stress triggering and stress memory observed from acoustic emission records in a salt mine, *Geophys. J. Int.* **182,** 933–948, doi: 10.1111/j.1365-246X.2010.04642.x.

Behlau, J., and G. Mingerzahn (2001). Geological and tectonic investigations in the former Morsleben salt mine (Germany) as a basis for the safety assessment of a radioactive waste repository, *Eng. Geol.* **61,** 83–97, doi: 10.1016/S0013-7952(01)00038-2.

Ben-Zion, Y., and P. Leary (1986). Thermoelastic strain in a half-space covered by unconsolidated material, *Bull. Seismol. Soc. Am.* **76,** 1447–1460.

Berger, J. (1975). A note on thermoelastic strains and tilts, *J. Geophys. Res.* **80,** 274–277.

Dieterich, J. (1994). A constitutive law for rate of earthquake production and its application to earthquake clustering, *J. Geophys. Res.* **99,** 2601–2618.

Dieterich, J., V. Cayol, and P. Okubo (2000). The use of earthquake rate changes as a stress meter at Kilauea volcano, *Nature* **408,** 457–460.

Eisenblätter, J., and T. Spies (2000). Ein Magnitudenmaß für Schallemissionsanalyse und Mikroakustik, in *Deutsche Gesellschaft für zerstörungsfreie Prüfung, 12. Kolloquium Schallemission*, Jena, Germany, 23–24 March 2000 (in German).

Fahland, S., R. Eickemeier, and T. Spies (2005). Bewertung von Gebirgsbeanspruchungen bei Verfüllmassnahmen im ERAM, in *5. Altbergbaukolloquium*, Clausthal-Zellerfeld, Germany, 3–5 November 2005 (in German).

Falls, S., and R. Young (1998). Acoustic emission and ultrasonic-velocity methods used to characterise the excavation disturbance associated with deep tunnels in hard rock, *Tectonophysics* **289,** 1–15.

Federal Office for Radiation Protection (2009). Stillegung ERA Morsleben, www.bfs.de/de/endlager/endlager_morsleben/stilllegung/genehmigungsverfahren/plan_sep_2009_rev_03_internet.pdf (last accessed November 2013) (in German).

Freed, A. M. (2005). Earthquake triggering by static, dynamic, and postseismic stress transfer, *Annu. Rev. Earth Planet. Sci.* **33,** 335–367.

Ge, M. (2005). Efficient mine microseismic monitoring, *Int. J. Coal Geol.* **64,** 44–56.

Gibowicz, S. J. (1989). Introduction, in *Mining Induced Seismicity*, S. J. Gibowicz (Guest Editor), special issue *Pure Appl. Geophys.* **129,** 283–284.

Gibowicz, S. J., and A. Kijko (1994). *An Introduction to Mining Seismology*, Academic Press, San Diego, California.

Harris, R. A. (1998). Introduction to special section: Stress triggers, stress shadows, and implications for seismic hazard, *J. Geophys. Res.* **103,** 24,347–24,358, doi: 10.1029/98JB01576.

Harris, R., and R. W. Simpson (1992). Changes in static stress on southern Californian faults after the 1992 Landers earthquake, *Nature* **360,** 251–254, doi: 10.1038/360251a0.

King, G., R. Stein, and J. Lin (1994). Static stress changes and the triggering of earthquakes, *Bull. Seismol. Soc. Am.* **84,** 935–953.

Köhler, N., T. Spies, and T. Dahm (2009). Seismicity patterns and variation of the frequency-magnitude distribution of microcracks in salt, *Geophys. J. Int.* **179,** 489–499, doi: 10.1111/j.1365-246X.2009.04303.x.

Lin, J., and R. Stein (2004). Stress triggering in thrust and subduction earthquakes, and stress interaction between the southern San Andreas and nearby thrust and strike-slip faults, *J. Geophys. Res.* **109,** no. B02303, doi: 10.1029/2003JB002607.

Maghsoudi, S., S. Cesca, S. Hainzl, D. Kaiser, D. Becker, and T. Dahm (2013). Improving the estimation of detection probability and magnitude of completeness in strongly heterogeneous media, an application to acoustic emission (AE), *Geophys. J. Int.* **193,** 1556–1569, doi: 10.1093/gji/ggt049.

Moriya, H., T. Fujita, H. Niitsuma, J. Eisenblätter, and G. Manthei (2006). Analysis of fracture propagation behavior using hydraulically induced acoustic emissions in the Bernburg salt mine, Germany, *Int. J. Rock Mech. Min. Sci.* **43,** no. 1, 49–57.

Naoi, M., M. Nakatani, Y. Yabe, G. Kwiatek, T. Igarashi, and K. Plenkers (2011). Twenty thousand aftershocks of a very small (M 2) earthquake and their relation to the mainshock rupture and geological structures, *Bull. Seismol. Soc. Am.* **101,** 2399–2407, doi: 10.1785/0120100346.

Okada, Y. (1992). Internal deformation due to shear and tensile faults in a half-space, *Bull. Seismol. Soc. Am.* **82,** 1018–1040.

Oye, V., H. Bungum, and M. Roth (2005). Source parameters and scaling relations for mining-related seismicity within the Pyhäsalmi ore mine, Finland, *Bull. Seismol. Soc. Am.* **95,** 1011–1026, doi: 10.1785/0120040170.

Prawirodirdjo, L., Y. Ben-Zion, and Y. Bock (2006). Observation and modeling of thermoelastic strain in SCIGN daily position time series, *J. Geophys. Res.* **111,** no. B02408, doi: 10.1029/2005JB003716.

Preuss, J., G. Eilers, and R. Mauke (2002). Post closure safety of the Morsleben repository, in *WM'02 Conference*, Tucson, Arizona, 24–28 February 2002.

Richardson, E., and T. H. Jordan (2002). Seismicity in deep gold mines of South Africa: Implications for tectonic earthquakes, *Bull. Seismol. Soc. Am.* **92,** 1766–1782, doi: 10.1785/0120000226.

Scholz, C. (2002). *Mechanics of Earthquakes and Faulting*, Cambridge University Press, Cambridge, England.

Schultz, R. (2000). Growth of geologic fractures into large-strain populations: Review of nomenclature, subcritical crack growth, and some implications for rock engineering, *Int. J. Rock Mech. Min. Sci.* **37,** 403–411.

Spies, T., and J. Eisenblätter (1999). Micro- and macrofracturing at the boundary of rock salt and anhydrite, in *Proc. 9th Int. Congr. Rock Mechanics, Paris*, A.A. Balkema, Rotterdam, The Netherlands, 1071–1074.

Spies, T., and J. Eisenblätter (2001). Acoustic emission investigation of microcrack generation at geological boundaries, *Eng. Geol.* **61,** 181–188, doi: 10.1016/S0013-7952(01)00053-9.

Stein, R. S. (1999). The role of stress-transfer in earthquake occurrence, *Nature* **402,** 605–609.

Toda, S., R. Stein, K. Richards-Dinger, and S. Bozkurt (2005). Forcasting the evolution of seismicity in southern California: Animations built on earthquake stress transfer, *J. Geophys. Res.* **110,** no. B05S16, doi: 10.1029/2004JB003415.

Toda, S., R. Stein, and T. Sagiya (2002). Evidence from the AD 2000 Izu island earthquake swarm that stressing rate governs seismicity, *Nature* **419,** 58–61.

Trifu, C. I. (2002). Introduction, in *Induced Seismicity*, C. I. Trifu (Editor), special issue *Pure Appl. Geophys.* **159,** 1–5.

Trifu, C. I. (2010). Introduction, in *Monitoring Induced Seismicity*, C. I. Trifu (Editor), special issue *Pure Appl. Geophys.* **167,** 1–3.

Vallejos, J., and S. McKinnon (2011). Correlation between mining and seismicity for re-entry protocol development, *Int. J. Rock Mech. Min. Sci.* **48,** 616–625.

Young, R., and D. S. Collins (1999). Monitoring an experimental tunnel seal in granite using acoustic emission and ultrasonic velocity, in *Rock Mechanics for Industry*, B. Amadei, R. L. Kranz, G. A. Scott, and P. H. Smeallie (Editors), *Proc. of the 37th International Conference on Ground Control in Mining*, Vail, Colorado, 6–9 June 1999, A.A. Balkema, Rotterdam, 869–876.

Young, R., S. Maxwell, T. Urbancic, and B. Feignier (1992). Mining-induced microseismicity: Monitoring and applications of imaging and source mechanism techniques, *Pure Appl. Geophys.* **139,** 697–719.

Institute of Geophysics
Hamburg University
Bundesstr. 55
20146 Hamburg, Germany
dirk.becker@zmaw.de
(D.B.)

Institute of Geological Sciences
Free University Berlin
Malteserstr. 74-100
12249 Berlin, Germany
(B.C.)

Federal Institute for Geosciences and Natural Resources
Stilleweg 2
30655 Hannover, Germany
(D.K.)

Section Physics of Earthquakes and Volcanoes
GFZ German Research Centre for Geosciences
Helmhotzstr. 6/7
14467 Potsdam, Germany
(T.D.)

Manuscript received 6 November 2013;
Published Online 15 July 2014